Normalization and Interpretation of Radar Images

J. Paul Skinner, Brian M. Kent, *Senior Member, IEEE*, Ronald C. Wittmann, *Senior Member, IEEE*, Dean L. Mensa, *Senior Member, IEEE*, and Dennis J. Andersh, *Member, IEEE*

***Abstract*— Calibrated radar images are often quantified as radar cross section. This interpretation, which is not strictly correct, can lead to misunderstanding of test target scattering properties. To avoid confusion, we recommend that a term such as "scattering brightness" (defined below) be adopted as a standard label for image-domain data.**

***Index Terms*— Radar imaging.**

I. Introduction

RADAR IMAGE data have often been represented as "*radar cross section (RCS) in* dBsm." Although images may properly have the units dB (re 1 m^2) (commonly abbreviated dBsm), the interpretation of image levels as RCS is incorrect except under special circumstances. Unfortunately, even legitimate labeling of image levels with dBsm can induce an unintentional connection between images and RCS data [1].

Images cannot, in general, be directly associated with RCS. Consider the effects of shadowing, for example. Here, the prominence of a scattering center depends on the influence of other parts of the target. A definition of RCS based on image data obviously cannot describe an intrinsic property of the component scatterer. The interpretation of image level as RCS can be justified only for targets consisting of isolated, independent[1], isotropic, nondispersive scattering centers. Such targets exist only in an approximate sense, at best.

Images are formed from weighted sums of scattering data over a range of frequencies and/or angles. If the weights are dimensionless, the image-domain function will have the same dimension as the original data. The problem arises in the interpretation of these weighted averages as RCS, a term reserved to describe target scattering for a specific frequency and geometry. Analysts familiar with the imaging process will most likely appreciate the distinction between RCS and images; other users of images, however, may interpret the units to imply a strict equivalence to RCS. To avoid confusion, we recommend that a term such as "scattering brightness" be adopted as a standard label for image magnitude. The definition and interpretation of scattering brightness are discussed below.

Manuscript received December 5, 1996; revised November 4, 1997.

J. P. Skinner is with the Department of Electrical and Computer Engineering, Air Force Institute of Technology, Wright-Patterson Air Force Base, OH 45433 USA.

B. M. Kent is with the Signature Technology Office, Air Force Research Laboratory, Wright-Patterson Air Force Base, OH 45433 USA.

R. C. Wittmann is with the National Institute of Standards and Technology, Boulder, CO 80303 USA.

D. L. Mensa was with the U. S. Naval Weapons Center, Pt. Mugu, CA 93042 USA.

D. J. Andersh is with Demaco Inc., Champaign, IL 61820 USA.

Publisher Item Identifier S 0018-926X(98)02740-9.

[1]That is, the target scatting matrix is the sum of the scattering matrices of the component scatterers.

II. Radar Cross Section and Scattering Matrix

Radar cross section (RCS) is defined as

$$\sigma(\boldsymbol{k}_s, \boldsymbol{k}_i) = \lim_{r\to\infty} 4\pi r^2 \frac{|E_s(\boldsymbol{k}_s)|^2}{|E_i(\boldsymbol{k}_i)|^2} \tag{1}$$

where E_i is the amplitude [V/m] of the incident plane wave field and E_s is the amplitude of the scattered field component received at a distance r from the target. RCS depends on the directions of incidence ($\hat{\boldsymbol{k}}_i$) and scattering ($\hat{\boldsymbol{k}}_s$) and on the frequency ($\omega = 2\pi f = kc, k = |\boldsymbol{k}_s| = |\boldsymbol{k}_i|$). Polarization dependence is suppressed in this discussion. In the monostatic case, $\boldsymbol{k}_s = -\boldsymbol{k}_i$.

Calibrated coherent radars usually measure (components of) the scattering matrix, which can be defined through the far-field relation

$$S(\boldsymbol{k}_s, \boldsymbol{k}_i) = \lim_{r\to\infty} r\exp(jkr)\frac{E_s(\boldsymbol{k}_s)}{E_i(\boldsymbol{k}_i)}. \tag{2}$$

As normalized here, S has the dimensions of length [m]. From (1) and (2)

$$\sigma(\boldsymbol{k}_s, \boldsymbol{k}_i) = 4\pi|S(\boldsymbol{k}_s, \boldsymbol{k}_i)|^2. \tag{3}$$

The target scattering matrix S is often determined from measurements using

$$\begin{aligned} S(\boldsymbol{k}_s, \boldsymbol{k}_i) &= \frac{F^{\text{target}}(\boldsymbol{k}_s, \boldsymbol{k}_i) - F^{bkgd}(\boldsymbol{k}_s, \boldsymbol{k}_i)}{F^{\text{ref}}(\boldsymbol{k}_s, \boldsymbol{k}_i) - F^{bkgd}(\boldsymbol{k}_s, \boldsymbol{k}_i)} S^{\text{ref}}(\boldsymbol{k}_s, \boldsymbol{k}_i) \\ &\equiv [F^{\text{target}}(\boldsymbol{k}_s, \boldsymbol{k}_i) - F^{bkgd}(\boldsymbol{k}_s, \boldsymbol{k}_i)]\kappa(k). \end{aligned} \tag{4}$$

(This calibration scheme requires measurement of the reference target at the test target location. Other schemes are possible.) We assume that $S^{\text{ref}}(\boldsymbol{k}_s, \boldsymbol{k}_i)$ is known from a previous measurement or computation. The F terms symbolize the complex response of the radar receiver, which is proportional to the scattered field in a linear system. Equation (4) uses background subtraction to remove clutter effects. Nominally, the calibration factor $\kappa(k)$ does not depend on the angles of incidence or scattering; it is commonly measured as a function of frequency in some advantageous fixed geometry.

III. Image Formation

A set of scattering data can produce a variety of images depending on the processing scheme. For example a "complex

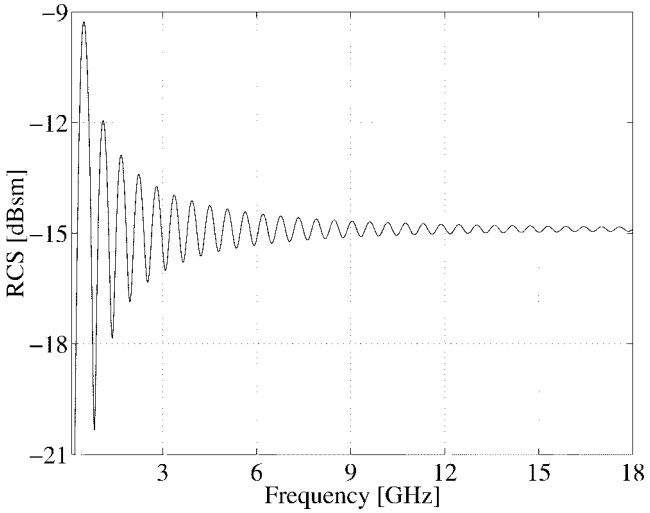

Fig. 1. Scattering data for an 8-in-diameter sphere: RCS versus frequency.

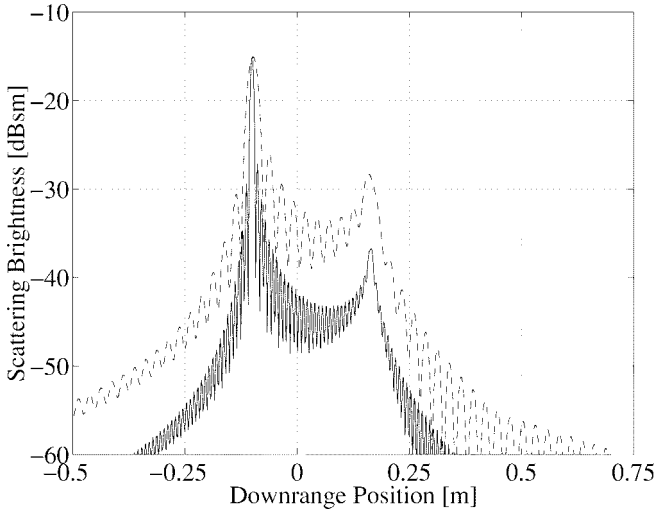

Fig. 2. Downrange image of a perfectly conducting 8-in sphere. Band 0.1–6 GHz (dashed). Band 0.1–18 GHz (solid). Normalized Kaiser–Bessel window ($\beta = 0$).

image function" $G(\boldsymbol{r})$ can be defined as

$$G(\boldsymbol{r}) \equiv \sqrt{4\pi} \sum_{\boldsymbol{k}_s, \boldsymbol{k}_i} w(\boldsymbol{k}_s, \boldsymbol{k}_i) S(\boldsymbol{k}_s, \boldsymbol{k}_i) \exp[-j(\boldsymbol{k}_s - \boldsymbol{k}_i) \cdot \boldsymbol{r}] \tag{5}$$

where both the magnitude (which is proportional to frequency) and the directions of $\boldsymbol{k}_s$ and $\boldsymbol{k}_i$ are allowed to vary. Images are basically averages (over frequency and/or direction) of *coherent* scattering data weighted by a function $w(\boldsymbol{k}_s, \boldsymbol{k}_i)$ usually selected to improve dynamic range at the expense of resolution or vice versa. The choice of weighting function can profoundly affect the resulting image.

To see how an image is formed, consider the case of isotropic nondispersive objects, which we call elementary targets (ET's) for convenience. By isotropic and nondispersive, we mean that there is a natural coordinate system in which the scattering matrix is independent of angle and frequency (over the parameter range of interest)

$$S_0(\boldsymbol{k}_s, \boldsymbol{k}_i) = S_0 = \text{constant}. \tag{6}$$

The origin of this coordinate system defines the mathematical location of the ET. If an ET is placed at position $\boldsymbol{\rho}$ in the test target coordinate system, the scattering matrix is

$$S(\boldsymbol{k}_s, \boldsymbol{k}_i) = S_0 \exp[j(\boldsymbol{k}_s - \boldsymbol{k}_i) \cdot \boldsymbol{\rho}] \tag{7}$$

where, as before, S_0 is independent of $\boldsymbol{k}_s$ and $\boldsymbol{k}_i$. In the test-target coordinate system, the scattering matrix has a *position-dependent* phase factor that is neither isotropic nor nondispersive. According to (3), (5), and (7), the image of an ET is

$$\begin{aligned} |G(\boldsymbol{r})|^2 &= \sigma \left| \sum_{\boldsymbol{k}_s, \boldsymbol{k}_i} w(\boldsymbol{k}_s, \boldsymbol{k}_i) \exp[-j(\boldsymbol{k}_s - \boldsymbol{k}_i) \cdot (\boldsymbol{r} - \boldsymbol{\rho})] \right|^2 \\ &= \sigma \, \mathrm{PSF}(\boldsymbol{r} - \boldsymbol{\rho}). \end{aligned} \tag{8}$$

Thus, the image is the point-spread function

$$\mathrm{PSF}(\boldsymbol{r}) \equiv \left| \sum_{\boldsymbol{k}_s, \boldsymbol{k}_i} w(\boldsymbol{k}_s, \boldsymbol{k}_i) \exp[-j(\boldsymbol{k}_s - \boldsymbol{k}_i) \cdot \boldsymbol{r}] \right|^2 \tag{9}$$

scaled by the RCS and appropriately translated. (The weighting function is generally selected so that the point-spread function is sharply peaked at $r = 0$.)

More complex targets are often modeled as collections of scattering centers. Interpretation of image levels to deduce the RCS of scattering centers is questionable unless these scattering centers approximate ET's. Even for targets that may be reasonably represented as assemblages of ET's such an interpretation is problematic. For example, intratarget interactions can produce shadows and ghosts. Also, because the point-spread function has nonzero width, the images of closely spaced scattering centers may interfere strongly. *In general, there is no simple connection between image levels and RCS.*

The prescription of images through (5) is actually quite inclusive. When $\boldsymbol{k}_s$ and $\boldsymbol{k}_i$ are fixed in direction and only frequency is varied, we obtain "downrange" images. When frequency is fixed and directions are varied, we obtain synthetic aperture radar (SAR) or inverse SAR (ISAR) images [2]. More generally, any combination of frequency and angular diversity is permitted.

IV. Definition of Scattering Brightness

Let us require that weights be dimensionless and normalized so that

$$\max_{\boldsymbol{r}} |\mathrm{PSF}(\boldsymbol{r})| = 1. \tag{10}$$

We propose to define an image function by

$$\mathcal{I}(\boldsymbol{r}) \equiv 10 \log_{10} |G(\boldsymbol{r})|^2 \tag{11}$$

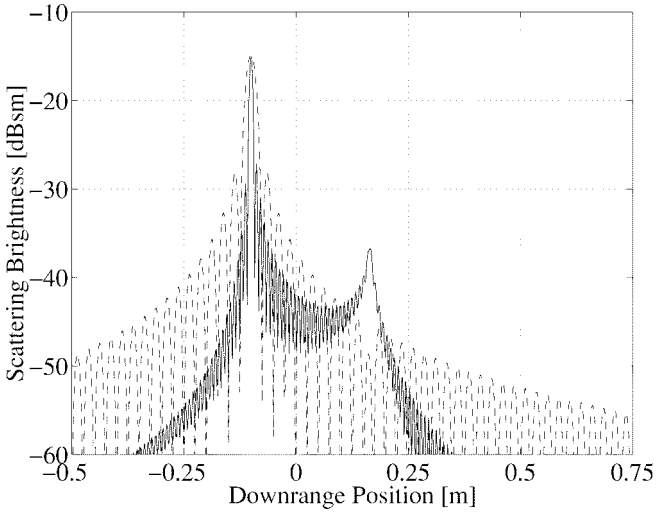

Fig. 3. Downrange image of a perfectly conducting 8-in sphere. Band 12–18 GHz (dashed). Band 0.1–18 GHz (solid). Normalized Kaiser–Bessel window ($\beta = 0$).

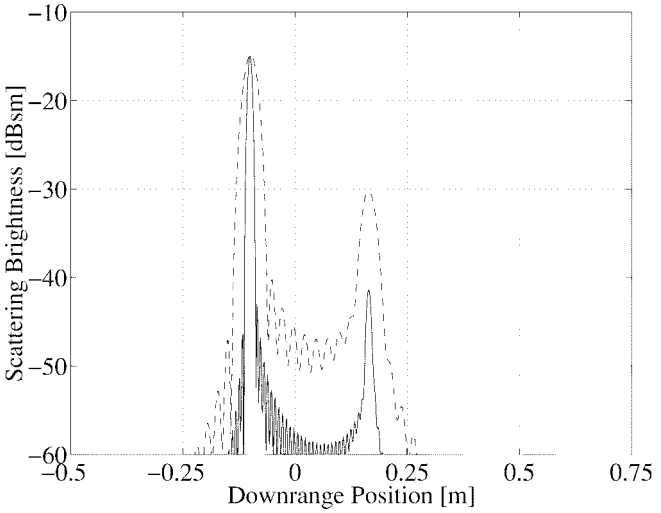

Fig. 4. Downrange image of a perfectly conducting 8-in sphere. Band 0.1–6 GHz (dashed). Band 0.1–18 GHz (solid). Normalized Kaiser–Bessel window ($\beta = 4$).

and to label image levels as scattering brightness with units dB (re 1 m^2) or dBsm.

Calibration is such that the image of an ET (with RCS σ) is proportional to the point-spread function and peaks at a scattering brightness of $10\log_{10}(\sigma)$ dBsm. To completely specify an image formed using the definition (5), the weighting function and the polarizations of incident and scattered fields must also be given. *Scattering brightness is not RCS.*

V. Imaging Example

As an illustration of the difference between RCS and scattering brightness, consider monostatic scattering from a perfectly electrically conducting sphere. The RCS of such a sphere is given exactly by the well-known Mie series [3] and the high-frequency limit is $\sigma_{\mathrm{hf}} = \pi a^2$, $ka \gg 1$, where a is the radius of the sphere. At high frequencies, the sphere is a good approximation of an ET since its RCS is approximately nondispersive. However, when ka is not much greater than unity, the RCS of the sphere becomes a strong function of frequency and it is this dispersive behavior that distinguishes the sphere from an ET. In Fig. 1, the RCS of a 0.2032-m (8-in) diameter sphere is plotted as a function of frequency over the range 0.1–18 GHz. It is convenient to interpret the frequency response of the sphere as an interference pattern between a nondispersive specular signal and a "creeping wave" signal whose amplitude decays with increasing frequency [4].

To form a one-dimensional downrange image, we let $\boldsymbol{r} = x\hat{\boldsymbol{x}}, \boldsymbol{k}_s = -\boldsymbol{k}_i = k\hat{\boldsymbol{x}}$ and sample monostatic scattering data at $N+1$ equally spaced frequencies. (Assume, for completeness, that the incident plane wave is y polarized and that the y polarized component of the scattered field is received.) The weighting function $w(\boldsymbol{k}_s, \boldsymbol{k}_i) = w(k_n)$ is chosen to be a normalized Kaiser–Bessel window ([5])

$$w(k_n) = C\mathrm{I}_0\left[\beta\sqrt{1-\left(\frac{2k_n - k_0 - k_N}{k_0 + k_N}\right)^2}\right] \Big/ \mathrm{I}_0(\beta) \tag{12}$$

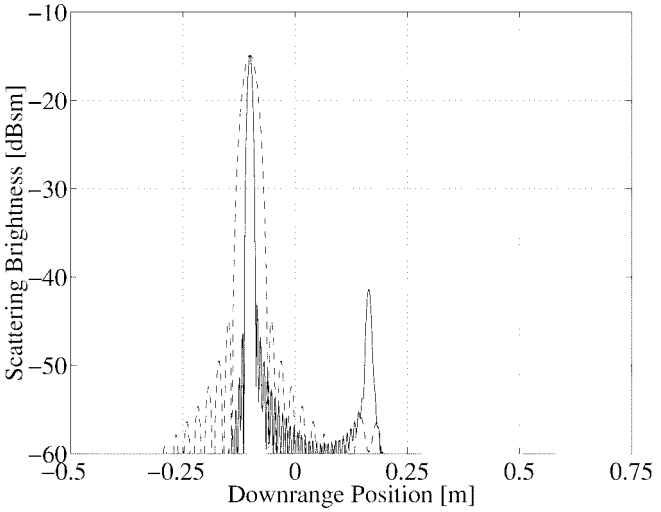

Fig. 5. Downrange image of a perfectly conducting 8-in sphere. Band 12–18 GHz (dashed). Band 0.1–18 GHz (solid). Normalized Kaiser–Bessel window ($\beta = 4$).

where $0 \le n \le N, \mathrm{I}_0$ is a modified Bessel function, β is a fixed parameter, $k_0(k_N)$ corresponds to the smallest (largest) frequency used, and C is a constant chosen so that (10) is satisfied. Then, according to (5) and (11), the scattering brightness $\mathcal{I}(x) \equiv \mathcal{I}(\boldsymbol{r})$ is given by

$$\mathcal{I}(x) = 10\log_{10}\left[4\pi\left|\sum_{n=0}^{N} w(k_n)S(k_n)\exp(-j2k_n x)\right|^2\right]. \tag{13}$$

The images (scattering brightness versus downrange position) plotted in Figs. 2 and 3 are each formed from a different frequency band and overlaid with the image formed from the

full 0.1–18-GHz band ($\Delta k = 2\pi\Delta f/c, \Delta f = 10$ MHz). The Kaiser–Bessel parameter β is set to zero, corresponding to a rectangular window. The specular portion of the RCS is evident at the same position in each image. Furthermore, the amplitude of this specular peak is independent of bandwidth and nearly equal to σ_{hf}. As such, the specular peak behaves like the peak from an ET. The creeping wave portion of the response produces a ghost image, which is evident at a position $(1+\pi/2)a = 0.26$ m behind the specular peak and, which has *an amplitude that depends on the frequency band*. The 0.1–6-GHz image in Fig. 2 shows the creeping wave peak about 14 dB below the specular peak, while for the 12–18-GHz image in Fig. 3, the creeping wave peak is hidden among the sidelobes of the specular peak.

The images plotted in Figs. 4 and 5 are identical to those in Fig.s 2 and 3, except that the Kaiser–Bessel parameter β is set to four. Changing the window shape does not visibly affect the specular peak position or amplitude, though it does affect the amplitude of the creeping wave peak. (Because of lower sidelobes of the $\beta = 4$ window, the specular and creeping wave responses do not overlap as strongly as they do in the $\beta = 0$ case. Viewed as a set, Figs. 2–5 show that the amplitude of the specular peak is nearly independent of the bandwidth and window shape function used to form the image, but these factors do affect the amplitude of the creeping wave peak. Clearly, it is not possible to assign a unique RCS value to the creeping wave peak from a downrange image! The important point to be made from this example is that the interpretation of image data as RCS is a problem, even for such a "simple" object as a sphere.

VI. Conclusions

The observations presented in this paper can be summarized as follows.

- Radar images are formed from weighted averages of coherent scattering data.
- Images can be properly represented with units of dBsm.
- However, image levels cannot be interpreted as RCS.
- The practice of labeling image levels as "scattering brightness [dBsm]" is recommended to prevent direct association with RCS.

Acknowledgment

The authors would like to thank Dr. W. J. Kent, Jr., Dr. G. Wilson, and Capt. W. D. Wood, Jr., for their helpful comments and technical support.

References

[1] J. P. Skinner, B. M. Kent, R. C. Wittmann, D. L. Mensa, and D. J. Andersh, "Radar image normalization and interpretation," in *Proc. Antenna Measurement Tech. Assoc.*, Boston, MA, Nov. 1997, pp. 303–307.

[2] D. L. Mensa, *High Resolution Radar Cross-Section Imaging*. Boston, MA: Artech House, 1991.

[3] L. B. Felsen and N. Marcuvitz, *Radiation and Scattering of Waves*. Englewood Cliffs, NJ: Prentice-Hall, 1973, p. 701.

[4] E. M. Kennaugh and D. L. Moffatt, "Transient and impulse response approximations," *Proc. IEEE*, vol. 53, pp. 893–900, Aug. 1965.

[5] A. V. Oppenheim and R. W. Schafer, *Discrete-Time Signal Processing*. Englewood Cliffs, NJ: Prentice-Hall, 1989.

J. Paul Skinner received the B.S. degree from Texas A&M University, College Station, in 1982, the M.S.E.E. degree from the Air Force Institute of Technology (AFIT), Wright-Patterson AFB, OH, in 1984, and the Ph.D. degree from The Ohio State University, Columbus, in 1991, all in electrical engineering.

From 1991 to 1996, he was on the faculty of the Department of Electrical and Computer Engineering at AFIT. Currently a Major in the United States Air Force, he serves on the staff of the Secretary of the Air Force at the Pentagon. He is an adjunct Associate Professor for AFIT.

Brian M. Kent (S'78–M'84–SM'93) received the B.S. degree in electical engineering (highest honors) from Michigan State University, East Lansing, in 1980, and the M.S. and Ph.D. degrees from The Ohio State University, Columbus, in 1981 and 1984, respectively

Since 1976, he has been employed by the Department of the Air Force, Wright-Patterson Air Force Base (WPAFB), OH. In 1985, he became the Senior Technical Expert for the Signature Technology Office, Air Force Research Laboratory, WPAFB. His specialties include reduced signature antennas and phased arrays, electromagnetic computations, and wide-band indoor and outdoor RCS measurements.

Dr. Kent is past chair of the Department of Defense RCS Measurements Working Group and the past chair of the Dayton Section IEEE APS/MTT Chapter. He is the current chair of the Department of Defense Range Commander's Council Signature Measurement and Standards Group (RCC/SMSG). At The Ohio State University, he won the award for Best Dissertation in Electrical Engineering (1984). He is the two-time recipient of the Air Force Avionics Samual Burka Award, three-time recipient of the Air Force Notable Achievement Award, and has two USAF letters of Commendation. In 1991, he was elected a Wright Laboratory Fellow. He is a member of Eta Kappa Nu, Phi Kappa Phi, and Tau Beta Pi.

Ronald C. Wittmann (M'88–SM'98) received the B.S. degree from the University of Washington, Seattle, in 1972, and the M.S. degree in physics from the University of Colorado, Boulder, in 1976.

Since 1978, he has been employed by the Electromagnetic Fields Division of the National Institute of Standards and Technology, Boulder, CO. His research has been in remote sensing, near-field antenna measurements, and RCS measurements.

Dean L. Mensa (S'79–M'80–SM'88) received the B.S. and M.S. degrees from the University of California, Los Angeles, in 1962 and 1964, respectively, and the Ph.D. degree in electrical engineering from the University of California, Santa Barbara, in 1980.

From 1976 to 1994, he was a Senior Technologist at the Naval Air Warfare Center, Point Mugu, CA, where he directed technical operations of the Radar Reflectivity Laboratory for 18 years. Currently a consultant, he has 35 years of experience in the analysis of airborne radar systems, radar target signatures, and RCS reduction. He is the author of more than 150 technical reports, many technical papers, and the books *High Resolution Radar Imaging* (Norwood, MA: Artech House, 1981) and *High Resolution Radar Cross-Section Imaging* (Norwood, MA: Artech House, 1991). His recent experience has been in the application of high-resolution microwave imaging.

Dr. Mensa received the Ventura County Chapter Sigma-Xi Award for Outstanding Research in 1982 and the Navy Meritorious Civilian Service Award in 1994.

Dennis J. Andersh (S'79–M'80) received the M.S. degree from the Air Force Institute of Technology, Wright-Patterson AFB, OH, in 1991.

With over 22 years experience in radar system development and operational fielding and usage, he was involved in directing electromagnetic research and development in the United States Air Force (USAF) for ground, air, and space applications. Since 1996 he has been a Senior Engineer for DEMACO, Inc., Champaign, IL, responsible for high-fidelity SAR scene modeling, multispectral target-signature simulations, and automatic target recognition (ATR) development for defense and commercial applications.

Mr. Andersh received the USAF Research and Development Award in 1994 for his work in asymptotic computational electromagnetics.